CYCLOTRON HARMONIC WAVE PROPAGATION AND INSTABILITIES: II. OBLIQUE PROPAGATION

by

J. A. Tataronis and F. W. Crawford

AEC Contract AT(04-3)326
(Project Agreement No. 1)

and

NASA Research Grant NGR 05-020-077

SU-IPR Report No. 326

June 1969

Institute for Plasma Research
Stanford University
Stanford, California

CYCLOTRON HARMONIC WAVE PROPAGATION AND INSTABILITIES: II. OBLIQUE PROPAGATION

by

J. A. Tataronis† and F. W. Crawford
Institute for Plasma Research
Stanford University
Stanford, California

ABSTRACT

Part I of this paper has discussed longitudinal wave propagation, perpendicular to the static magnetic field, in a warm homogeneous magnetoplasma. Part II extends the work to oblique propagation. The ring and Maxwellian transverse velocity distributions, which are absolutely unstable and stable, respectively, for perpendicular propagation, are shown here to be both absolutely unstable for oblique propagation. Their instabilities are radically affected by the introduction of axial velocity spread. A detailed study is made for the cases of a Maxwellian transverse distribution with resonance and resonance-squared axial velocity distributions. It is shown that absolute instabilities occur at high energy anisotropies. These become convectively unstable as the anisotropy is reduced, and are quenched as isotropy is approached. The isotropic Maxwellian is treated in detail, and shows both cyclotron and Landau collisionless damping.

† Now at CEN de Saclay, France

CONTENTS

LIST OF FIGURES

1. INTRODUCTION

In Part I (Tataronis and Crawford 1969), we considered the properties of perpendicularly propagating CHW for the ring, spherical shell, and Maxwellian electron velocity distributions, and for a mixture of ring and Maxwellian. We continue by considering oblique propagation. In Section 3, a thorough study of the ring distribution is made. This is followed by consideration in Section 4 of a Maxwellian transverse distribution. Though highly instrictive, these distributions are not realistic in the sense that the electrons in practical magnetoplasmas will always have some motions parallel to the static magnetic field. For this reason, the remainder of the paper is devoted to assessing the influence of such motions on the strength and nature of CHW instabilities. Section 5 retains the Maxwellian transverse distribution, and investigates the effects introduced by resonance and resonance-squared axial velocity distributions. This requires some refinements to the stability criterion used in Part I. These are presented in Section 2. Finally, Section 6 treats an isotropic Maxwellian distribution.

As before, we emphasize that we are not presenting a review of previous work, but are trying to present systematically in a single source the salient features emerging from our numerical studies of the very complicated CHW dispersion relations appropriate to a variety of basic electron velocity distributions. The pioneer work in the field, and many more recent results, should be accessible via the review by Crawford (1967).

2. THEORY

The general CHW dispersion relation may be written as (see Part I)

$$K(\omega,\underset{\sim}{k}) = 1 + \frac{\omega_p^2}{k^2} \sum_{n=-\infty}^{\infty} \int_{-\infty}^{\infty} dv_{\parallel} \frac{H_n(v_{\parallel})}{\omega - k_{\parallel} v_{\parallel} - n\omega_c} = 0 \qquad (\omega_i < 0) \quad ,$$

$$H_n(v_{\parallel}) = 2\pi \int_0^{\infty} dv_{\perp} \left(\frac{n\omega_c}{v_{\perp}} \frac{\partial f_0}{\partial v_{\perp}} + k_{\parallel} \frac{\partial f_0}{\partial v_{\parallel}} \right) J_n^2 \left(\frac{k_{\perp} v_{\perp}}{\omega_c} \right) v_{\perp} \quad . \qquad (1)$$

For velocity distributions of the form $f_0(v_{\perp},v_{\parallel}) = f_{\perp}(v_{\perp})\delta(v_{\parallel})$, (1) reduces to

$$K(\omega,\underset{\sim}{k}) = 1 - \frac{\omega_p^2}{\omega_c^2} \left[\frac{k_{\perp}^2}{k^2} \sum_{n=-\infty}^{\infty} p_n \frac{n\omega_c}{\omega - n\omega_c} + \frac{k_{\parallel}^2}{k^2} \sum_{n=-\infty}^{\infty} q_n \frac{\omega_c^2}{(\omega - n\omega_c)^2} \right] = 0 \quad ,$$

$$p_n = -2\pi \frac{\omega_c^2}{k_{\perp}^2} \int_0^{\infty} dv_{\perp} \frac{df_{\perp}(v_{\perp})}{dv_{\perp}} J_n^2 \left(\frac{k_{\perp} v_{\perp}}{\omega_c} \right) \quad , \quad q_n = 2\pi \int_0^{\infty} dv_{\perp} f_{\perp}(v_{\perp}) J_n^2 \left(\frac{k_{\perp} v_{\perp}}{\omega_c} \right) v_{\perp} \quad . \qquad (2)$$

Two such cases, i.e. without axial velocity spread, will be studied in Sections 3 and 4. It is clear from (2) that the roots $\omega(\underset{\sim}{k}$ real) must be either real, or occur in complex conjugate pairs. This is similar to the behavior of the cases treated in Part I. Mode coupling, and absolute instability, will again be shown to occur.

When there is axial velocity spread, the situation is more complicated, and it becomes important to note that $K(\omega,\underset{\sim}{k})$ given by (1) is not a unique function, but has two branches for $k_{\parallel}$ real. These are readily separated by introduction of the identity

$$\frac{1}{v_{\parallel} - w_n} = -i \int_0^{\mp\infty} d\zeta \, \exp[i(v_{\parallel} - w_n)\zeta] \quad , \qquad (3)$$

where $w_n = (\omega - n\omega_c)/k_{\parallel}$. To ensure convergence of the integral, the plus sign is chosen if $w_{ni} < 0$, and the negative if $w_{ni} > 0$. Substituting

(3) in (1), and assuming $\omega_i < 0$, leads to

$$K(\omega,\underset{\sim}{k}) = \begin{cases} K^+(\omega,k_\perp,k_\parallel) = 1 + 2\pi i \dfrac{\omega_p^2}{k_\parallel k^2} \displaystyle\sum_{n=-\infty}^{\infty} H_n^+(w_n,k_\perp,k_\parallel) & (k_\parallel > 0) \ , \\ K^-(\omega,k_\perp,k_\parallel) = 1 - 2\pi i \dfrac{\omega_p^2}{k_\parallel k^2} \displaystyle\sum_{n=-\infty}^{\infty} H_n^-(w_n,k_\perp,k_\parallel) & (k_\parallel < 0) \ , \end{cases}$$

$$H_n^+(w_n,k_\perp,k_\parallel) = \int_0^\infty \frac{d\zeta}{2\pi} \exp(-iw_n\zeta)\, \bar{H}_n(\zeta,k_\perp,k_\parallel) \ ,$$

$$H_n^-(w_n,k_\perp,k_\parallel) = \int_{-\infty}^0 \frac{d\zeta}{2\pi} \exp(-iw_n\zeta)\, \bar{H}_n(\zeta,k_\perp,k_\parallel) \ . \qquad (4)$$

Here, $\bar{H}_n(\zeta,k_\perp,k_\parallel)$ is the Fourier transform of $H_n(v_\parallel,k_\perp,k_\parallel)$,

$$\bar{H}_n(\zeta,k_\perp,k_\parallel) = \int_{-\infty}^{\infty} dv_\parallel \exp(iv_\parallel\zeta)\, H_n(v_\parallel,k_\perp,k_\parallel) \ . \qquad (5)$$

The two branches K^+, K^-, are connected by the relation

$$K^+(-\omega^*,k_\perp,k_\parallel) = K^-(\omega,k_\perp,-k_\parallel)^* \ . \qquad (6)$$

As a result of the decomposition of $K(\omega,k_\perp,k_\parallel)$ in (4), the instability criterion stated in Part I, Section 2, must be modified. The appropriate changes have been stated by Derfler (1967). For discussion, assume that $k_\perp$ is a fixed, real number and that the propagation is parallel to the magnetic field. Derfler's work then implies that absolute instability is present if zeros of $K^+(\omega,k_\perp,k_\parallel)$ collide across the positive $k_\parallel$ axis, or if zeros of $K^-(\omega,k_\perp,k_\parallel)$ collide across the negative $k_\parallel$ axis, as ω varies along some contour in the lower half complex plane. We shall make use of this modified instability criterion in later sections.

3. RING DISTRIBUTION

This distribution may be written as (see Part I)

$$f_0(v_\perp, v_\parallel) = \frac{1}{2\pi v_{0\perp}} \delta(v_\perp - v_{0\perp})\, \delta(v_\parallel) \quad . \tag{7}$$

Substitution of (7) in (2) yields the dispersion relation

$$K(\omega, \underset{\sim}{k}) = 1 - \frac{\omega_p^2}{\omega_c^2}\left[\frac{k_\perp^2}{k^2} \sum_{n=-\infty}^{\infty} \frac{1}{\mu_\perp} \frac{dJ_n^2(\mu_\perp)}{d\mu_\perp} \frac{n\omega_c}{\omega - n\omega_c} + \frac{k_\parallel^2}{k^2} \sum_{n=-\infty}^{\infty} J_n^2(\mu_\perp) \frac{\omega_c^2}{(\omega - n\omega_c)^2}\right] = 0 \quad . \tag{8}$$

Remembering that $k^2 = k_\perp^2 + k_\parallel^2$, (8) may be rearranged to give

$$\cot^2\theta = \frac{k_\parallel^2}{k_\perp^2} = - \frac{1 - \frac{\omega_p^2}{\omega_c^2} \sum_{n=-\infty}^{\infty} \frac{1}{\mu_\perp} \frac{dJ_n^2(\mu_\perp)}{d\mu_\perp} \frac{n\omega_c}{\omega - n\omega_c}}{1 - \frac{\omega_p^2}{\omega_c^2} \sum_{n=-\infty}^{\infty} J_n^2(\mu_\perp) \frac{\omega_c^2}{(\omega - n\omega_c)^2}} \quad , \tag{9}$$

where θ is the angle between $\underset{\sim}{k}$ and the static magnetic field.

Dispersion Characteristics

Figure 1 shows numerical solutions of (19) for several values of θ, and $\omega_p^2/\omega_c^2 = 1$. The curves for $\theta \neq 90^\circ$ indicate that there are now two branches undulating about each cyclotron harmonic line. At $n\omega_c$, there are resonances (all n), and cutoffs ($n \neq 0$). Two additional cutoffs can be located by putting $\mu_\perp = 0$ in (9),

$$\omega^2 = \frac{1}{2}\left\{\omega_p^2 + \omega_c^2 \pm \left[(\omega_p^2 - \omega_c^2)^2 + 4\omega_p^2\omega_c^2\sin^2\theta\right]^{\frac{1}{2}}\right\} \quad . \tag{10}$$

These tend to ω_p, ω_c, as θ tends to zero, and $(\omega_p^2+\omega_c^2)^{\frac{1}{2}}$, zero, as θ tends to 90°.

It is easy to see from (9) that the undulating branches cut the harmonic lines at the zeros of $J_n(\mu_\perp)$. As θ tends to 90°, the curves

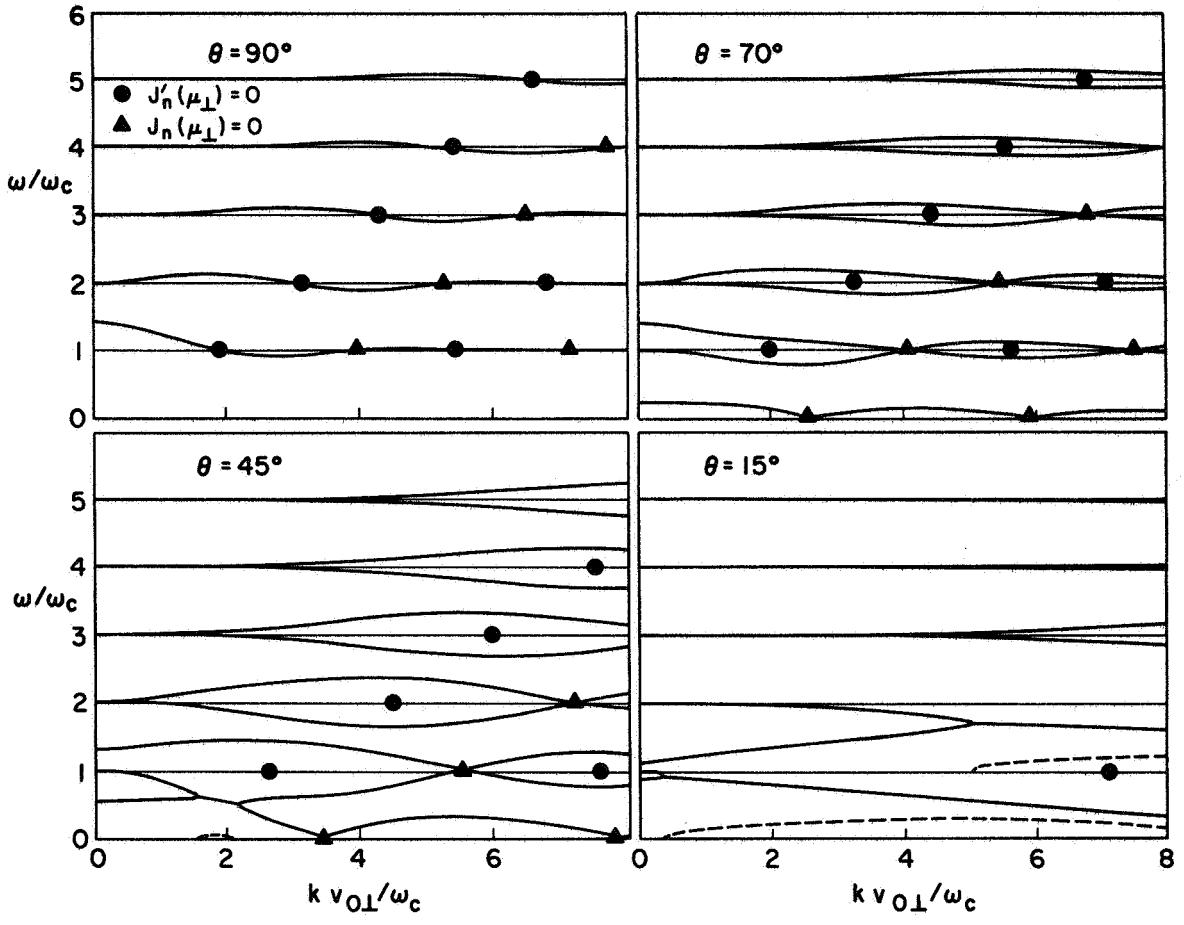

Fig. 1. DISPERSION CHARACTERISTICS OF OBLIQUELY PROPAGATING CYCLOTRON HARMONIC WAVES: RING DISTRIBUTION.

pinch towards the points $J_n'(\mu_\perp) = 0$, so that in the limit one undulating branch intersects each harmonic line at $J_n(\mu_\perp) = 0$ and $J_n'(\mu_\perp) = 0$. We note from the curves for $\theta = 45^\circ$ that a downgoing loop from $\omega/\omega_c = 1$ has coupled with an upgoing loop from $\omega/\omega_c = 0$ to produce an absolute instability. An additional instability is exhibited for $\theta = 15^\circ$, where for convenience ω_i/ω_c (dashed) has been plotted using $\omega/\omega_c = 1$ as a base line. We conclude from these results, and table 1 of Part I, that instability may occur in oblique propagation well below the threshold for unstable perpendicular propagation.

A thorough study of (9) could be made via diagrams such as figure 1. Since we are solving for $\omega(\underset{\sim}{k}$ real), and the instabilities are absolute, we have preferred the alternative of producing the families of curves shown in figure 2 for fixed $k_\perp$ and varying $k_\parallel$. These have the advantages of being easily related to the work of Part I, and are directly relevant to parallel propagation in a transversely bounded plasma, where the finite dimensions could be accounted for roughly by taking a fixed value of $k_\perp$.

To find the cutoffs for figure 2, we put $k_\parallel = 0$ in (9). One set of cutoffs are given by the zeros of the numerator, which is just the CHW dispersion relation for perpendicular propagation, so they may be read off figure 2 of Part I. Our choice of $\mu_\perp = k_\perp v_{0\perp}/\omega_c = 1, 3, 4.5$, will now be appreciated. The first value is in a region where no instability can occur for perpendicular propagation; the second is where only the zero-frequency instability can occur, and the third is where mode coupling can occur for $1 \le \omega_r/\omega_c \le 2$. A second set of cutoffs can be obtained by approximating (9) by

$$\frac{k_\parallel^2}{k_\perp^2} = -\frac{2n^2 J_n'(\mu_\perp)}{\mu_\perp J_n(\mu_\perp)}\left(\frac{\omega - n\omega_c}{n\omega_c}\right) \qquad (\omega \approx n\omega_c) \quad . \tag{11}$$

Thus, $\omega/\omega_c \to n$ as $k_\parallel \to 0$, so there is a cutoff at each cyclotron harmonic.

The resonances $(k_\parallel = \infty)$ occur when the denominator of (9) is zero. This function is plotted in figure 3a. For $\omega_p^2/\omega_c^2 = 0.25$, two branches

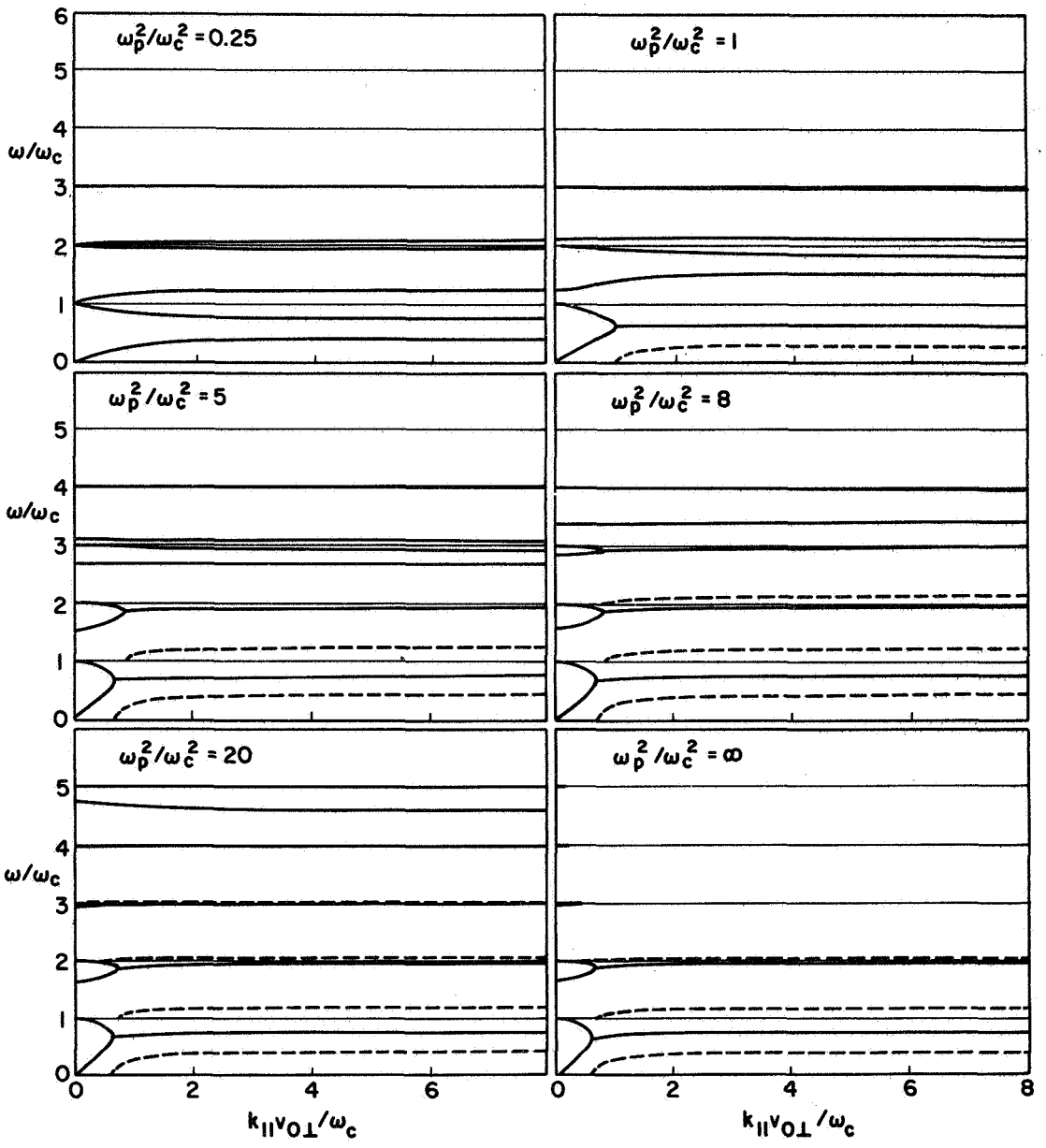

(a) $k_{\perp} v_{0\perp}/\omega_c = 1.0$

Fig. 2. DISPERSION CHARACTERISTICS OF OBLIQUELY PROPAGATING CYCLOTRON HARMONIC WAVES: RING DISTRIBUTION.

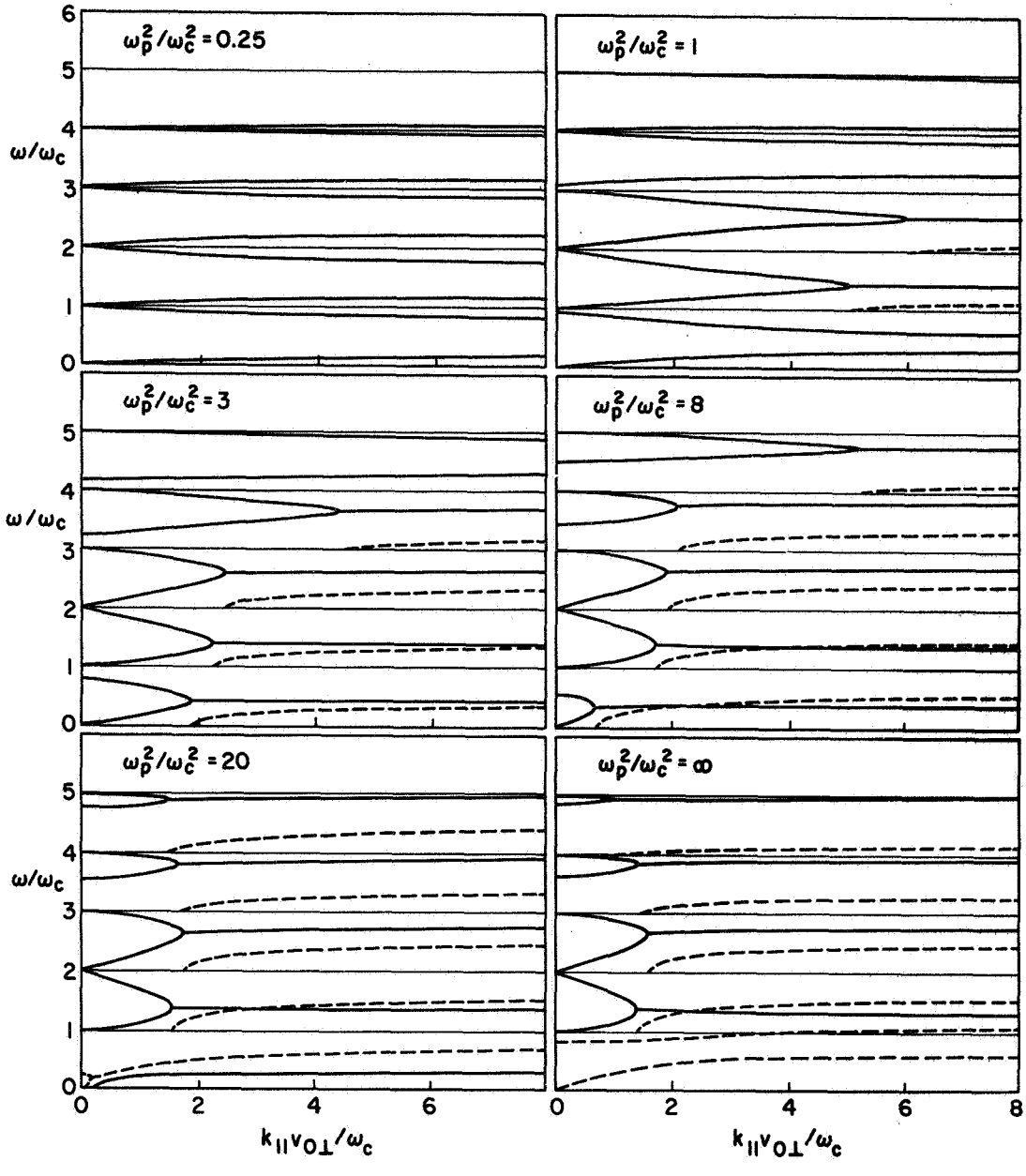

(b) $k_{\perp} v_{0\perp}/\omega_c = 3.0$

Fig. 2. CONTINUED.

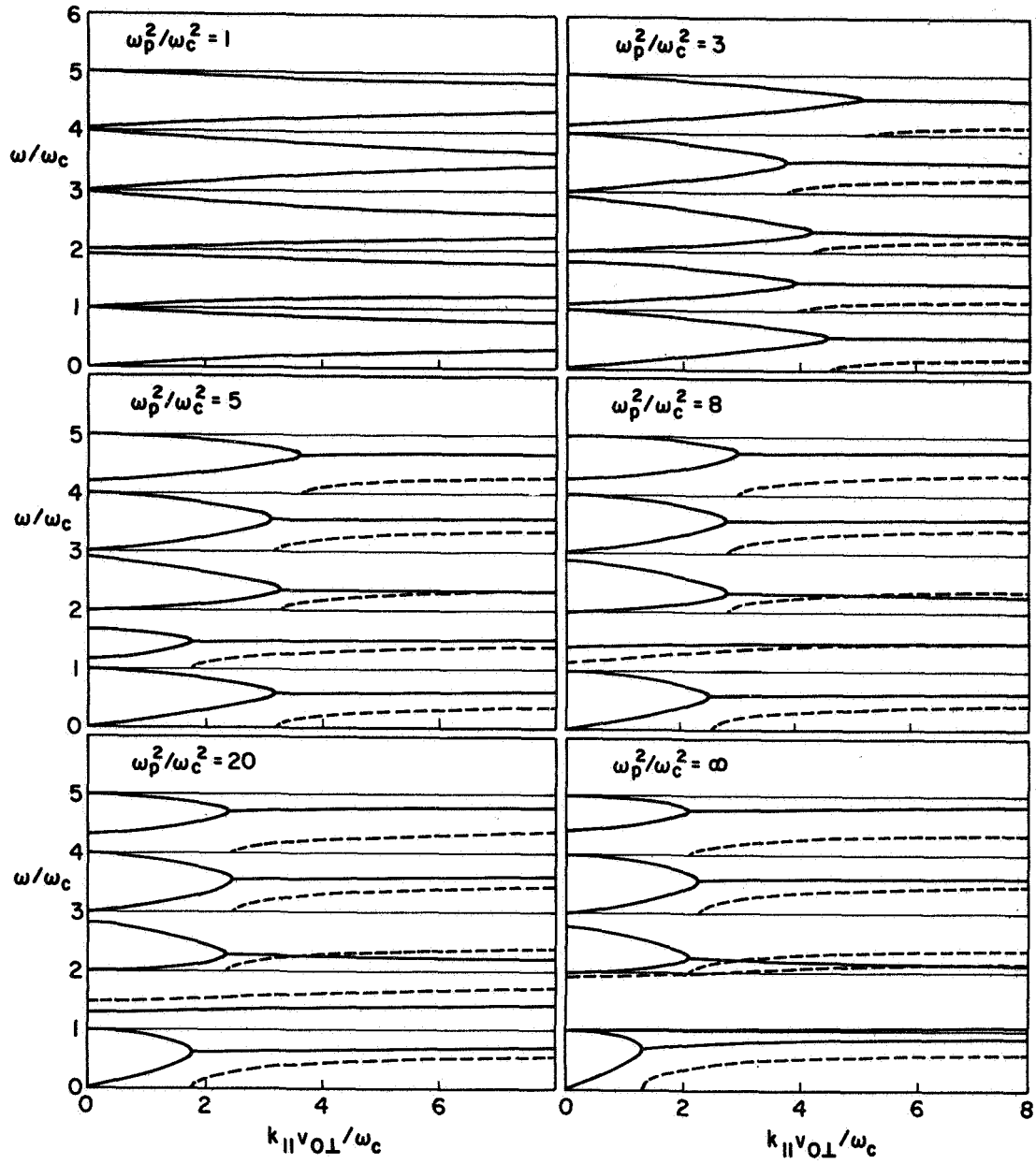

(c) $k_{\perp} v_{0\perp}/\omega_c = 4.5$

Fig. 2. CONTINUED.

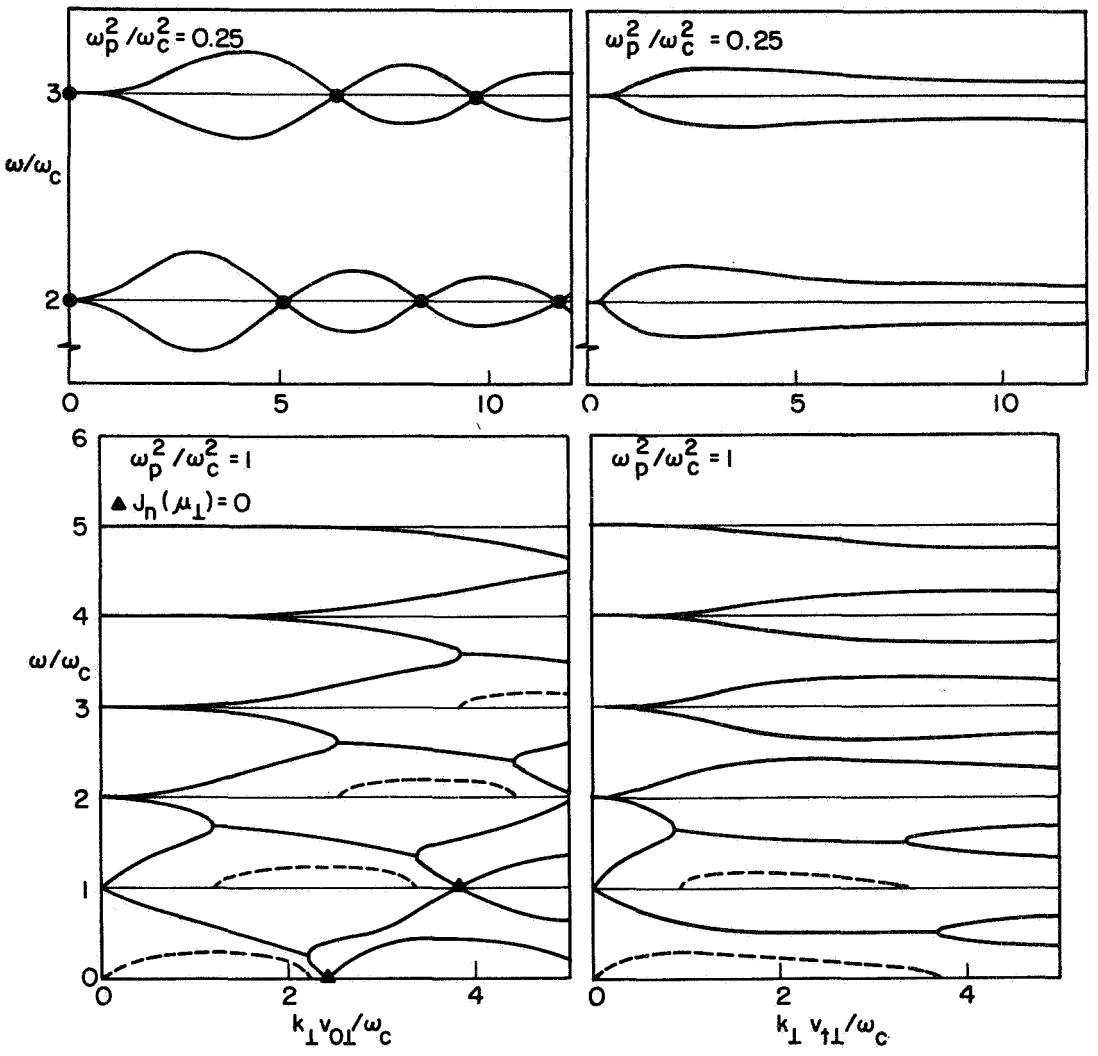

(a) Ring distribution

(b) Maxwellian transverse distribution

Fig. 3. RESONANCE FREQUENCIES ($k_\parallel = \infty$) OF OBLIQUELY PROPAGATING CYCLOTRON HARMONIC WAVES.

undulate about each harmonic line, and intersect them at the zeros (α_{nm}) of $J_n(\mu_\perp)$. There is no coupling between upgoing and downgoing loops, so the resonance frequencies are real. For $\omega_p^2/\omega_c^2 = 1$, coupling occurs. For all cases we have considered, coupling occurs in the ranges $\alpha_{nm} < \mu_\perp < \alpha_{(n+1),m}$ and $\alpha_{(n+1),m} < \mu_\perp < \alpha_{n,(m+1)}$, for ω_p^2/ω_c^2 sufficiently large. Some critical values of ω_p^2/ω_c^2 are given in table 1 for the first three frequency bands. They are clearly much lower than those for purely perpendicular propagation (see table 1 of Part I).

Frequency Band					
$0 < \omega/\omega_c < 1$		$1 < \omega/\omega_c < 2$		$2 < \omega/\omega_c < 3$	
Range of $\mu_\perp$	ω_p^2/ω_c^2	Range of $\mu_\perp$	ω_p^2/ω_c^2	Range of $\mu_\perp$	ω_p^2/ω_c^2
0 - 2.40	0.34	0 - 3.83	0.53	0 - 5.14	0.66
2.40 - 3.83	1.07	3.83 - 5.14	1.70	5.14 - 6.38	2.29
3.83 - 5.52	1.38	5.14 - 7.02	1.62	6.38 - 8.42	1.82

TABLE 1. Instability threshold values of ω_p^2/ω_c^2

We now consider the families of dispersion characteristics displayed in figure 2. For ω_p^2/ω_c^2 small, each passband has two propagation branches associated with it, the frequency spread about $n\omega_c$ decreasing rapidly with increasing n. For $\mu_\perp = 1$, instability first occurs in the lowest passband, for a value of $k_\parallel v_{0\perp}/\omega_c$ corresponding to propagation at $\theta \sim 45°$. Successive passbands become unstable roughly for $\omega_p^2 + \omega_c^2 > (n\omega_c)^2$, but the growth rates are small except in the first few passbands. For $\mu_\perp = 3$, instability occurs first in the second and third passbands, and for $\omega_p^2/\omega_c^2 = 3$ has spread to the first and fourth. Above $\omega_p^2/\omega_c^2 = 17.02$, we expect additional effects since the zero-frequency instability has set in for purely perpendicular propagation. These appear in the lowest passband for $\omega_p^2/\omega_c^2 = 20$. At small $k_\parallel$, there are two imaginary roots. As $k_\parallel$ increases, there is a transition to complex roots with a very rapid growth rate. Further increase in ω_p^2/ω_c^2 reduces the real parts to zero, leaving purely imaginary solutions for all $k_\parallel$. For the final case, $\mu_\perp = 4.5$, where unstable perpendicular propagation first occurs in the band $1 \le \omega_r/\omega_c \le 2$, the characteristics

in all other bands are similar to those for $\mu_\perp = 1$, though with stronger growth rates. In the second passband, however, there is absolute instability for all $k_\parallel$ once the perpendicular instability threshold has been passed. The results for $\omega_p^2/\omega_c^2 \geq 8$ suggest that the instability in this band always has the highest growth rate.

A common feature of the curves in figure 2 is that the branches $\omega(k_\parallel)$ increase or decrease monotonically towards coupling points. It follows that the threshold for coupling will have $k_\parallel = \infty$, and that curves such as those of figure 3 determine immediately whether a given band will be unstable or not. The instability thresholds suggested in this way are substantially lower than for perpendicular propagation. In anticipation of Section 4, it should be pointed out that, in practice, there is always a spread of electron velocities parallel to the magnetic field. This can strongly modify the threshold conditions. An additional caution should be stated against interpreting too literally the limit $k_\parallel \to \infty$, since the theory will ultimately break down at wavelengths comparable with an electronic Debye length.

4. MAXWELLIAN TRANSVERSE DISTRIBUTION: NO AXIAL VELOCITY

In Part I, it was established that introduction of a transverse velocity spread led to less violent perpendicularly propagating instability than that associated with a ring distribution, and could give complete stability if $\partial f_0/\partial v_\perp < 0$ for all $v_\perp > 0$. The Maxwellian falls into this class, and we now wish to determine whether stability persists when oblique propagation is considered.

For no axial velocity spread, the distribution may be written as

$$f_\perp(v_\perp, v_\parallel) = \frac{1}{2\pi v_{t\perp}^2} \exp\left(-\frac{v_\perp^2}{2v_{t\perp}^2}\right)\delta(v_\parallel) \quad . \tag{12}$$

Substitution in (2), and some manipulation, yields the dispersion relation

$$K(\omega, \underset{\sim}{k}) = 1 - \frac{\omega_p^2}{\omega_c^2} \sum_{n=-\infty}^{\infty} \frac{\exp(-\lambda) I_n(\lambda)}{\lambda k^2} \left[\frac{k_\perp^2 n\omega_c}{\omega - n\omega_c} + \frac{\lambda k_\parallel^2 \omega_c^2}{(\omega - n\omega_c)^2}\right] = 0 \quad , \tag{13}$$

where $\lambda = (k_\perp v_{t\perp}/\omega_c)^2$. Equation (13) may be rearranged analogously to (9) as

$$\cot^2\theta = \frac{k_\parallel^2}{k_\perp^2} = -\frac{1 - \dfrac{\omega_p^2}{\omega_c^2} \displaystyle\sum_{n=-\infty}^{\infty} \frac{\exp(-\lambda) I_n(\lambda)}{\lambda} \frac{n\omega_c}{\omega - n\omega_c}}{1 - \dfrac{\omega_p^2}{\omega_c^2} \displaystyle\sum_{n=-\infty}^{\infty} \exp(-\lambda) I_n(\lambda) \frac{\omega_c^2}{(\omega - n\omega_c)^2}} \quad . \tag{14}$$

Dispersion Characteristics

As for the ring distribution, one set of cutoffs are found from (14) at $n\omega_c$, and a second set are determined by the numerator. Its zeros are solutions of the CHW dispersion relation for perpendicular propagation, and can be read off figure 5 of Part I. Unlike the ring distribution, these cutoff frequencies are always real. Resonances occur at

zeros of the numerator of (14). Their behavior is shown in figure 3b, contrasted with that of the ring distribution. There are two modes in each passband, but instead of undulating about the harmonic lines, their separation increases to a maximum then decreases to zero as $k_\perp \to \infty$. Even for $\omega_p^2/\omega_c^2 = 1$, coupling is possible, and figure 3b shows absolute instability in the first two passbands. A consequence of the nonundulatory nature of the propagation branches is that there can be instability in only a single range of $k_\perp v_{t\perp}/\omega_c$, for a given passband. For distributions such as the ring, there may be many ranges.

Figure 4 shows typical dispersion characteristics computed from (14). They may be compared with the relevant curves of figure 2b for the ring distribution, and are found to be very similar. Although an exhaustive numerical study has not been made, we can be sure that there are no long wavelength $(k_\parallel \to 0)$ instabilities for any value of ω_p^2/ω_c^2. Our next concern must be to see to what extent the short wavelength instabilities are quenched by the introduction of axial velocity spread.

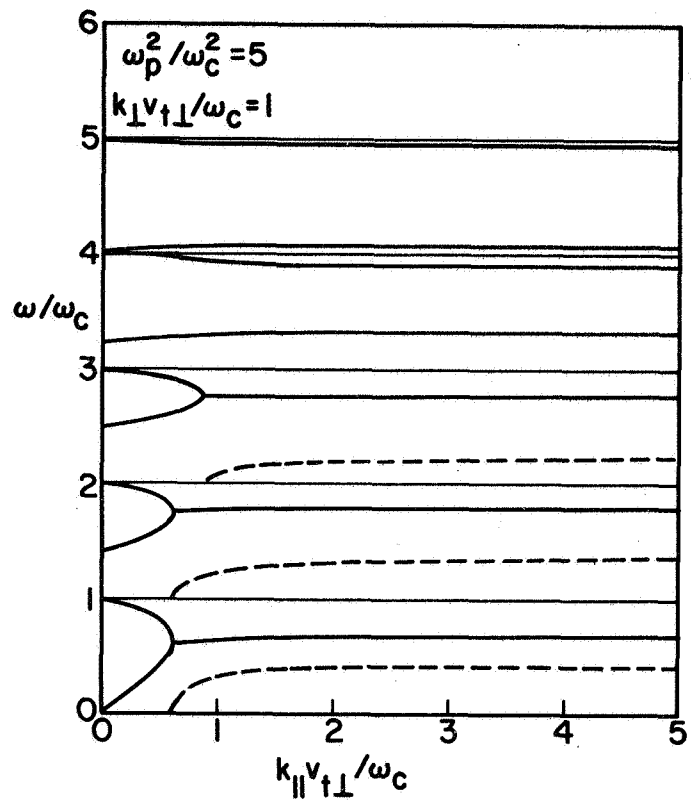

Fig. 4. DISPERSION CHARACTERISTICS OF OBLIQUELY PROPAGATING CYCLOTRON HARMONIC WAVES: MAXWELLIAN TRANSVERSE DISTRIBUTION. NO AXIAL VELOCITY.

5. MAXWELLIAN TRANSVERSE DISTRIBUTION: RESONANCE AXIAL DISTRIBUTION

To derive the CHW dispersion relation in the presence of a velocity spread parallel to the static magnetic field, (1) is required, and for axial distributions such as the Maxwellian leads to an expression transcendental in $k_\parallel$. The numerical stability analysis is then greatly complicated by the presence of an infinite series of Landau poles. These mathematical difficulties can be avoided, with little loss to the physics, by considering plausible analytic approximations to the axial velocity distribution of interest, constructed so as to yield simpler dispersion relations algebraic in $k_\parallel$, i.e. with a small number of Landau poles. For this reason, we shall now investigate resonance-type distributions of the forms

$$f_0(v_\perp, v_\parallel) = \frac{v_{t\parallel}}{2\pi^2 v_{t\perp}^2} \frac{\exp(-v_\perp^2/2v_{t\perp}^2)}{(v_\parallel^2 + v_{t\parallel}^2)} \quad , \quad f_0(v_\perp, v_\parallel) = \frac{v_{t\parallel}^3}{\pi^2 v_{t\perp}^2} \frac{\exp(-v_\perp^2/2v_{t\perp}^2)}{(v_\parallel^2 + v_{t\parallel}^2)^2} \quad . \tag{15}$$

Substitution of the first of these in (1) yields

$$K^+(\omega, \underset{\sim}{k}) = 1 - \frac{\omega_p^2}{\omega_c^2} F(\omega - ik_\parallel v_{t\parallel}, k_\perp, k_\parallel) \qquad (\omega_i < 0, \; k_\parallel > 0) \quad ,$$

$$F(\omega, k_\perp, k_\parallel) = \sum_{n=-\infty}^{\infty} \frac{\exp(-\lambda) I_n(\lambda)}{\lambda k^2} \left[\frac{k_\perp^2 n\omega_c}{\omega - n\omega_c} + \frac{\lambda k_\parallel^2 \omega_c^2}{(\omega - n\omega_c)^2} \right] \quad . \tag{16}$$

Substitution of the second ("resonance-squared") distribution in (1) leads to

$$K^+(\omega, \underset{\sim}{k}) = 1 - \frac{\omega_p^2}{\omega_c^2} \left[F(\omega - ik_\parallel v_{t\parallel}, k_\perp, k_\parallel) + ik_\parallel v_{t\parallel} \frac{\partial F(\omega - ik_\parallel v_{t\parallel}, k_\perp, k_\parallel)}{\partial \omega} \right] = 0 \quad ,$$

$$(\omega_i < 0, \quad k_\parallel > 0) \quad . \tag{17}$$

Stability Analysis

Comparison of (16) with (13) shows that the dispersion relation for the simple resonance axial distribution can be obtained directly from that with no axial velocity by replacing ω with $\omega - ik_{\parallel} v_{t_{\parallel}}$. Since the initial step in the stability analysis is to solve (16) for $\omega(\underset{\sim}{k} \text{ real})$, we see that the transformation changes ω_i, but not ω_r. Figure 5 illustrates this for the parameters of figure 4. Both of the imaginary parts of the complex ω solutions are plotted. The real parts are still given by figure 4. We note that the introduction of the complex Doppler shift due to axial velocities has the effect of stabilizing the short wavelengths $(k_{\parallel} \to \infty)$. In the first passband, there is now only a narrow range of $k_{\parallel} v_{t\perp}/\omega_c$ for which $\omega_i < 0$. In the second passband, the range is even more restricted. The third passband has been stabilized, and all higher passbands $(3 < \omega_r/\omega_c)$ show the same attenuation, $\omega_i = k_{\parallel} v_{t_{\parallel}}$.

In previous sections, and Part I of the paper, complex conjugate solutions were obtained for $\omega(\underset{\sim}{k} \text{ real})$, and the instabilities were interpretable as absolute. With an axial velocity spread, this is no longer the case, and more detailed stability analysis is required. This could be carried out for the simple resonance distribution, but we shall not do so, since it has the undesirable feature of an infinite thermal velocity. We have employed it because of the direct demonstration it provides, and the insight it gives, into the stabilizing effect of axial velocities. For the stability analysis, we shall consider the dispersion relation of (17), for the resonance-squared distribution. This has a thermal velocity of $v_{t_{\parallel}}$.

Figure 6 shows typical dispersion characteristics computed from (17) for the parameters of figure 4. As in our previous examples, there are two propagating branches in each passband. For clarity, these have been separated into two sets. We note that there is one unstable branch in the first passband, with $\omega_i/\omega_c < 0$ over a short range of $k_{\parallel} v_{t_{\parallel}}/\omega_c$, and a root with ω_i/ω_c dipping down towards instability in the second passband.

The latter is studied in more detail in the conformal mappings of figure 7, which show contours A-D in the complex ω-plane mapped into the complex $k_{\parallel}$-plane via (17). In accordance with the stability criterion

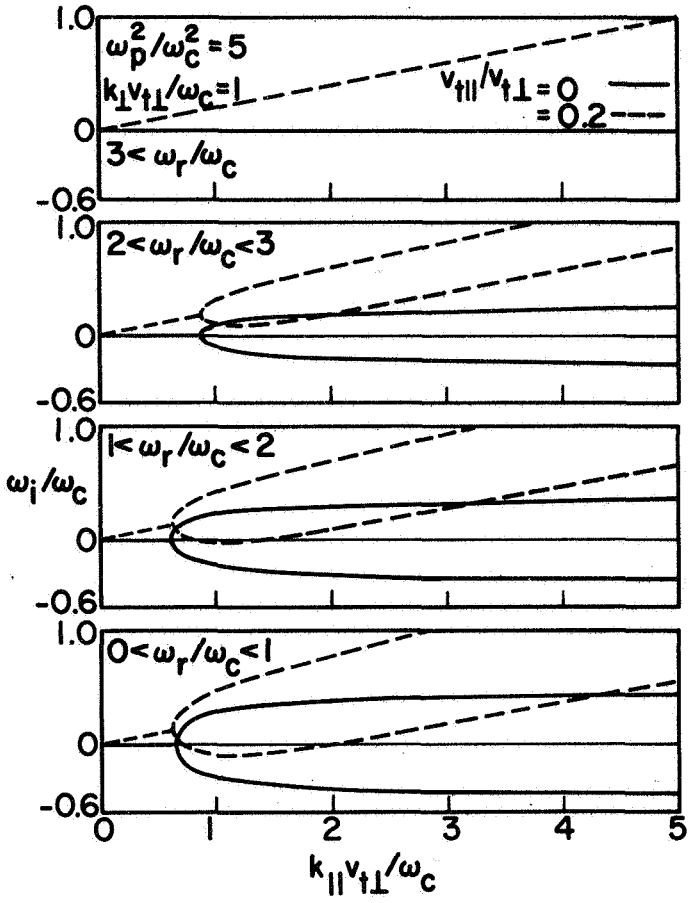

Fig. 5. DISPERSION CHARACTERISTICS OF OBLIQUELY PROPAGATING CYCLOTRON HARMONIC WAVES: MAXWELLIAN TRANSVERSE DISTRIBUTION. RESONANCE AXIAL DISTRIBUTION.

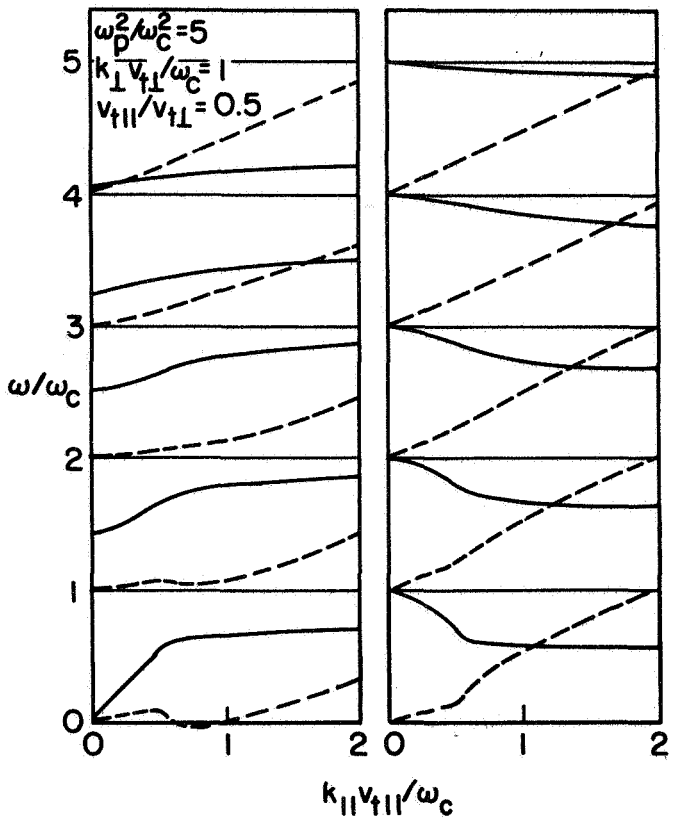

Fig. 6. DISPERSION CHARACTERISTICS OF OBLIQUELY PROPAGATING CYCLOTRON HARMONIC WAVES: MAXWELLIAN TRANSVERSE DISTRIBUTION. RESONANCE-SQUARED AXIAL DISTRIBUTION.

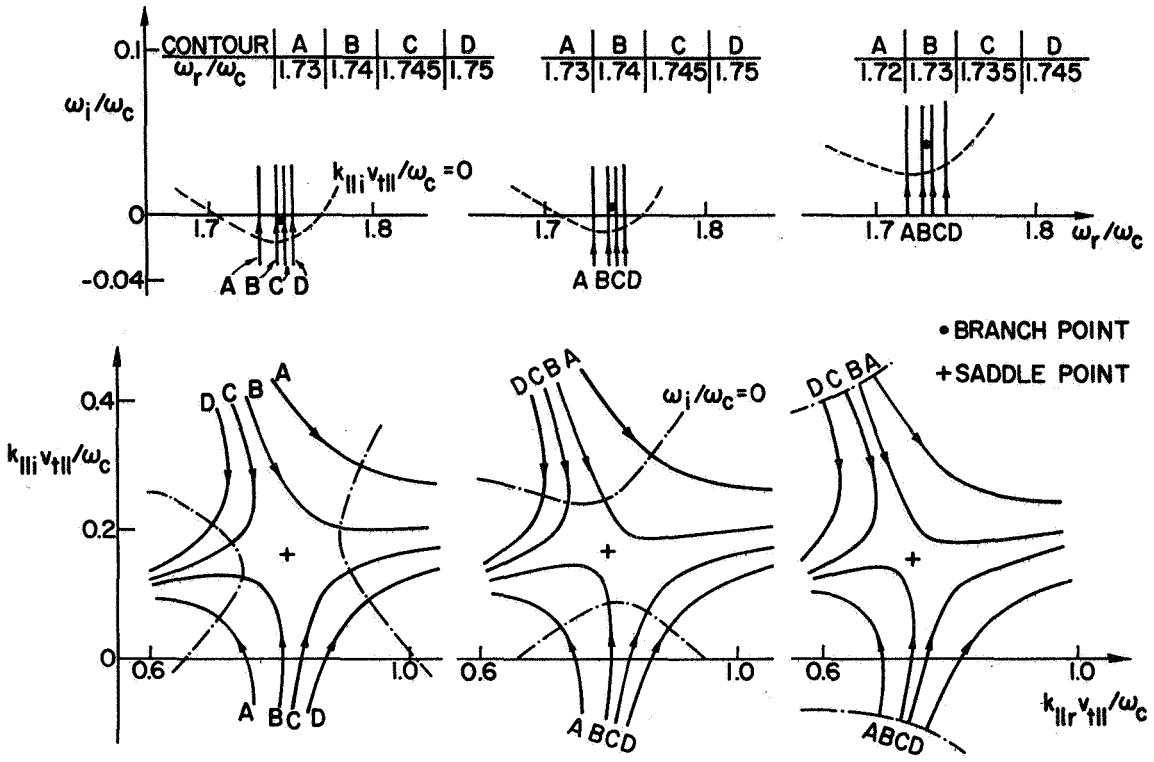

(a) $v_{t_\|}/v_{t_\perp} = 0.42$ (b) $v_{t_\|}/v_{t_\perp} = 0.43$ (c) $v_{t_\|}/v_{t_\perp} = 0.50$

Fig. 7. STABILITY ANALYSIS OF OBLIQUELY PROPAGATING CYCLOTRON HARMONIC WAVES: MAXWELLIAN TRANSVERSE DISTRIBUTION. RESONANCE-SQUARED AXIAL DISTRIBUTION.

quoted in Section 2, we look for saddlepoints $(\partial K^+/\partial k_\parallel = 0)$ corresponding to the merging of two zeros of $K^+(\omega,\underset{\sim}{k})$ across the positive $k_\parallel$ axis, and their corresponding branchpoints in the ω-plane. For $v_{t\parallel}/v_{t\perp} = 0.42$, merging occurs with $\omega_i < 0$ at the branchpoint, so there is absolute instability. An increase to $v_{t\parallel}/v_{t\perp} = 0.43$ makes $\omega_i > 0$ at the branchpoint. Since there are still solutions with $\omega_i < 0$ for $k_{\parallel i} v_{t\parallel}/\omega_c = 0$, the situation is now convectively unstable. For a further increase, to $v_{t\parallel}/v_{t\perp} = 0.50$, we see that $\omega_i > 0$ for $k_{\parallel i} v_{t\parallel}/\omega_c = 0$. This implies that the convective instability has been quenched and the root is stable. There would still remain of course, the unstable root shown in the first passband in figure 6. This could be removed by a further increase in $v_{t\parallel}/v_{t\perp}$.

To complete the stability analysis, it would be necessary to fix $v_{t\parallel}/v_{t\perp}$ and repeat the procedure for all real $k_\perp$. We will not do this, but will simply state the following speculative general conclusions, which are supported by other computations we have carried out on this and other magnetoplasma instabilities: Oblique propagation always leads to absolute instability if there is zero axial velocity spread, i.e. infinite anisotropy. As the anisotropy is reduced, the instabilities become convective. They are finally quenched as isotropy is approached.

6. ISOTROPIC MAXWELLIAN DISTRIBUTION

To complete the comparison with the basic cases treated in Part I, we now consider a Maxwellian transverse velocity distribution, and a Maxwellian axial distribution. Most generally, this may be written as

$$f_0(v_\perp, v_\parallel) = \frac{1}{(2\pi)^{3/2} v_{t_\parallel} v_{t_\perp}^2} \exp\left(- \frac{v_\perp^2}{2v_{t_\perp}^2} - \frac{v_\parallel^2}{2v_{t_\parallel}^2} \right) , \tag{18}$$

where $v_{t_\parallel}$ and $v_{t_\perp}$ are the parallel and perpendicular thermal velocities, respectively. Substitution in (1) leads to the dispersion relation

$$K(\omega, \underset{\sim}{k}) = 1 + \frac{\omega_p^2}{k^2 v_{t_\parallel}^2} \left[1 + \sum_{n=-\infty}^{\infty} \exp(-\lambda) I_n(\lambda) \frac{\omega - (1-T) n\omega_c}{2^{\frac{1}{2}} k_\parallel v_{t_\parallel}} Z\left(\frac{\omega - n\omega_c}{2^{\frac{1}{2}} k_\parallel v_{t_\parallel}} \right) \right] = 0 , \tag{19}$$

where $T = v_{t_\parallel}^2 / v_{t_\perp}^2$, and $Z(z)$, which arises from the $v_\parallel$ integration, is defined as (Fried and Conte 1961)

$$Z(z) = \frac{1}{\pi^{\frac{1}{2}}} \int_{-\infty}^{\infty} \frac{\exp(-t^2)}{t - z} \, dt - i\sigma \pi^{\frac{1}{2}} \exp(-z^2) \quad \begin{cases} \sigma = 0 , & z_i < 0 \\ = 1 , & = 0 \\ = 2 , & > 0 \end{cases} . \tag{20}$$

Here, the principal part of the integral is taken if z lies on the real t axis.

For anisotropic plasmas with $v_{t_\parallel} < v_{t_\perp}$, instabilities similar to those discussed in Section 5 are to be expected. They have attracted considerable interest, and the reader is referred to the literature (see Crawford 1968 for references). Here we shall consider the isotropic case ($v_t = v_{t_\parallel} = v_{t_\perp}$), which is completely stable (Bernstein 1958).

Dispersion Characteristics

Figure 8 shows numerical solutions $\omega(\underset{\sim}{k}$ real) to (19), and confirms the absence of instability. As in all other cases in Part II,

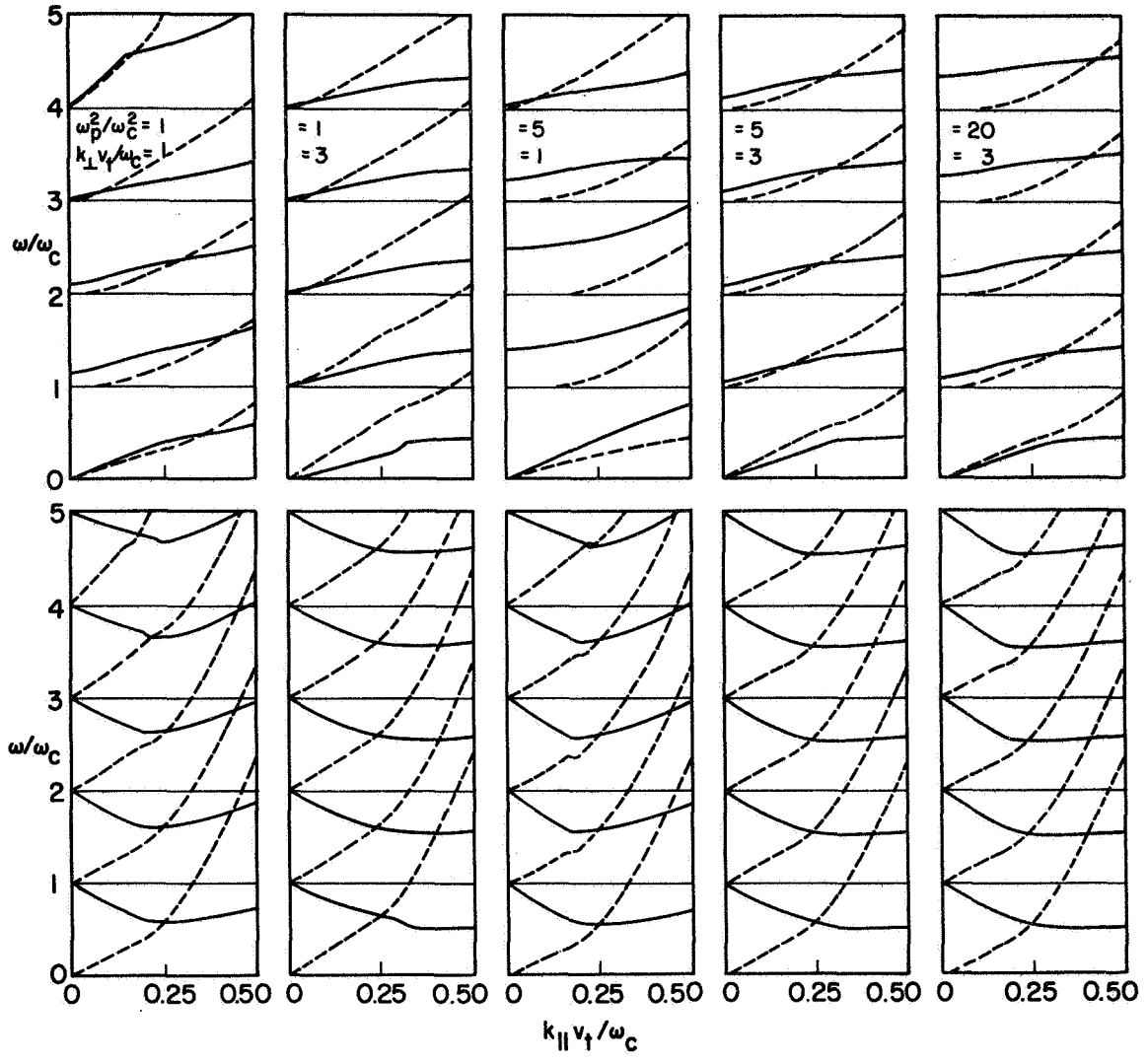

Fig. 8. DISPERSION CURVES FOR OBLIQUELY PROPAGATING CYCLOTRON HARMONIC WAVES: ISOTROPIC MAXWELLIAN DISTRIBUTION.

there are two branches in each passband. These have been separated, for clarity. Although there is no collisionless damping for purely perpendicular propagation, we note that the attenuation increases very rapidly with $k_{\|} v_t/\omega_c$, particularly for the modes with cutoffs at $n\omega_c$. Bearing in mind that $\omega_i \approx \omega_r$ corresponds to an attenuation of over 50 dB/cyclotron period $(= 2\pi/\omega_c)$, it will be appreciated from figure 8 that propagation will be difficult to observe experimentally for angles only a few degrees off exact perpendicularity.

Since there are no absolute instabilities present, we are entitled to solve (19) for $\underset{\sim}{k}(\omega$ real). The character of the Z-function of (20) makes this by no means trivial, however, and for complex $\underset{\sim}{k}$ we shall present only the set of curves shown in figure 9. Particular branches have been chosen so as to illustrate the passage from no collisionless damping in the limit $\theta = 90^\circ$, to Landau damping of plasma oscillations when $\theta = 0$. A distinction may be made in this respect between cyclotron and Landau-type interactions: An electron spiralling about the magnetic field sees the wave at the Doppler-shifted frequency $\omega - k_{\|} v_{\|}$. If a spread in $v_{\|}$ exists, it is possible to find electrons for which $\omega' \approx n\omega_c$, where n is an integer. There is then an energy exchange between the electrons and the CHW via its electric field. Damping results if the electrons gain energy, while instability occurs if the electrons lose energy. Cyclotron damping (or instability) arises from those electrons which see the CHW at $n\omega_c$ $(n \neq 0)$. If the electrons see a static field, corresponding to $n = 0$, Landau damping (or instability) results. In the limiting case $\theta = 0$, the electric field of the wave is parallel to $\underset{\sim}{B}_0$, so the damping is purely of the Landau type.

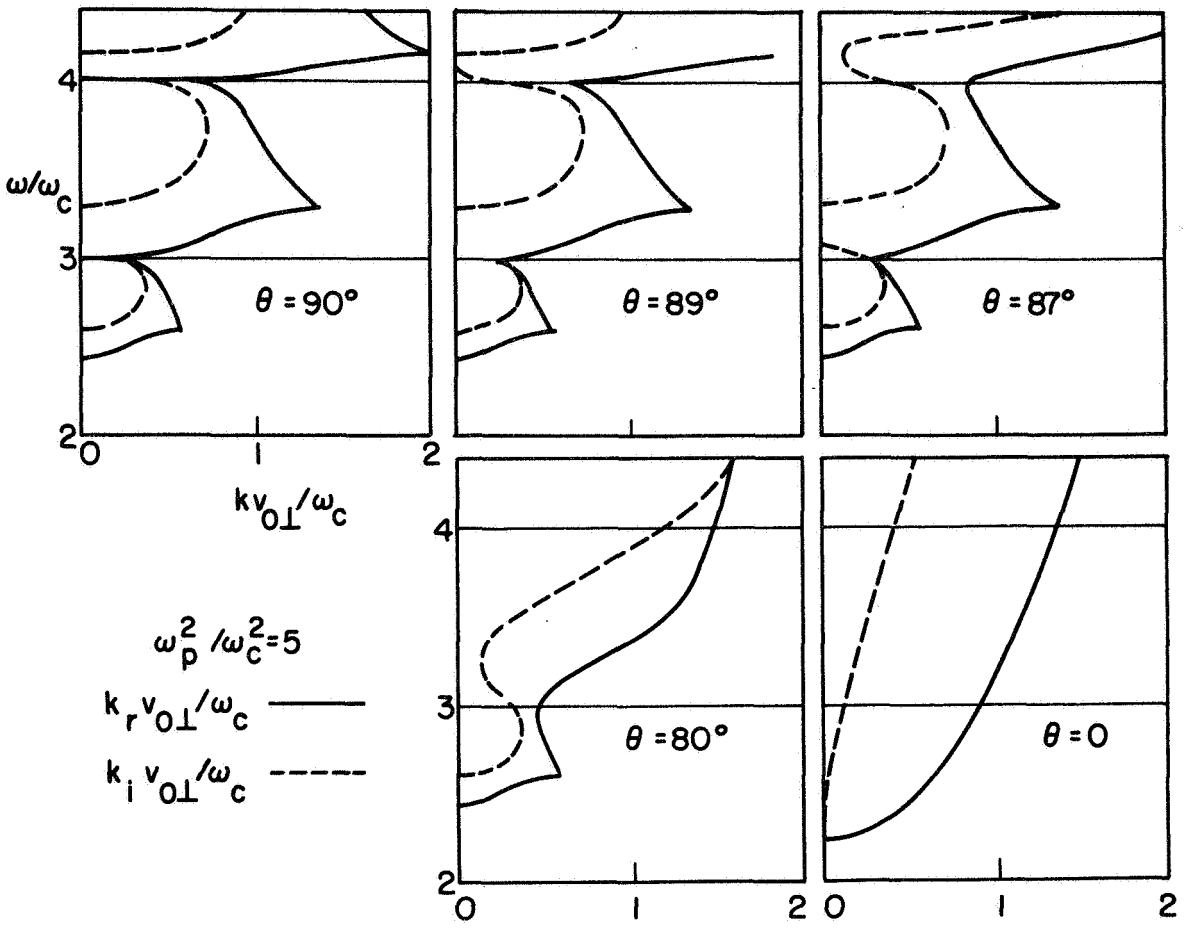

Fig. 9. DISPERSION CURVES FOR OBLIQUELY PROPAGATING CYCLOTRON HARMONIC WAVES: ISOTROPIC MAXWELLIAN DISTRIBUTION.

7. DISCUSSION

The computations of Sections 3-6 demonstrate that oblique propagation has features which disappear in the perpendicular propagation limit. Most important is the presence of a second branch in each cyclotron harmonic band. These contribute materially to mode coupling and the occurrence of instabilities. For the ring distribution, the results of Section 3 indicate much lower instability thresholds (ω_p^2/ω_c^2), while Section 4 demonstrates that instability can occur in oblique propagation for the Maxwellian transverse distribution; a distribution which was shown in Part I to be stable for perpendicular propagation.

Addition of an axial velocity distribution produces successively three new effects. First, it stabilizes short wavelength instabilities. Second, it can convert absolute to convective instability, and third it can quench instabilities entirely if isotropy is approached. Indeed, the dispersion relation for an isotropic Maxwellian generally shows very strong damping, except within a few degrees of exactly perpendicular propagation.

In Part I, a mixture of ring and Maxwellian distributions was examined in detail. It would be very time-consuming and expensive to extend this work to oblique propagation, but we may speculate on the likely behavior of this and other mixtures of energetic electrons in a stable background. It seems likely that the high damping in a Maxwellian plasma could only be offset by a relatively dense energetic group, and that marginal stability would occur for nearly perpendicular propagation. Further work is required, and may point the way to a suitable experiment for checking the theory. For example, the density of the energetic group could be raised while oblique CHW propagation was measured in a Maxwellian background plasma. The reduction of damping and the onsets of convective and absolute instability should all be measurable for comparison with numerical predictions.

This work was supported by the U.S. Atomic Energy Commission, and the National Aeronautics and Space Administration. The authors are indebted to Dr. H. Derfler for many helpful discussions.

REFERENCES

Bernstein, I. B. 1958 Phys. Rev. 109, 10.

Crawford, F. W. 1968 Paper in A Survey of Phenomena in Ionized Gases. Vienna: IAEA.

Derfler, H. 1967 Phys. Letters 24A, 763.

Fried, B. D., and Conte, S. D. 1961 The Plasma Dispersion Function. New York: Academic Press.

Tataronis, J. A., and Crawford, F. W. 1969 SU-IPR Report No. 325.

AEC DISTRIBUTION LIST

Raymond F. Askew
Dept. of Physics
Auburn University
Auburn, Ala. 36830

Peter Auer
Upson Hall
Cornell University
Ithaca, N.Y. 14850

David E. Baldwin
Dept. of Engrg & Applied Science
Mason Labs, 400 Temple St.
Yale University
New Haven, Conn. 06520

A. Banos
University of Calif., L.A.
Dept. of Physics
Los Angeles, Calif 90024

George Bekefi
Research Lab of Electronics
MIT
Cambridge, Mass. 02138

Ira B. Bernstein
Dept. of Engrg and Applied Science
Yale University
Mason Labs
400 Temple St.
New Haven, Conn. 06520

C. K. Birdsall
EE Dept. & Computer Sciences
Cory Hall
Univsity of Calif.
Berkeley, Calif. 94720

S. C. Brown
Research Lab of Electronics
MIT
Cambridge, Mass. 02138

Oscar Buneman - SEL
Stanford University
Stanford, Calif. 94305

Chia-Kun Chu
Columbia University
Dept. of Mech. Engrg.
New York, N.Y. 10027

Kun-Mo Chung
Polytechnic Inst. of Brooklyn
333 Jay Street
Farmingdale, N.Y. 11201

Frederick W. Crawford - SEL
Stanford University
Stanford, Calif. 94305

E. E. Donaldson
Dept. of Physics
Wash. State University
Pullman, Wash. 99163

William E. Drummond
Dept. of Physics
Univ. of Texas
Austin, Texas 78712

Gordon H. Dunn
Natl. Bur. of Standards
Joint Institute for Lab Astrophysics
1511 Univ. Ave.
Boulder, Colo. 80304

Burton D. Fried
Dept. of Physics
Univ. of Calif., L.A.
Los Angeles, Calif. 90024

Charles R. Finfgeld
Asst. Prof. of Physics
Roanoke College
Salem, Va. 24153

Harold Grad
Magneto-Fluid Dynamics Div
Inst. of Math. Studies -
New York Univ.
4 Wash. Place
New York, N.Y. 10013

Hans R. Griem
Dept. of Physics and Astronomy
Univ. of Maryland
College Park, Md. 20742

Robert A. Gross
School of Engrg & Appl. Science
Columbia University
236 S.W. Mudd Bldg.
New York, N.Y. 10027

Gregory Haas
Dept. of Physics
Univ. of Houston
3801 Chillen Blvd.
Houston, Texas 77004

E. G. Harris
Dept. of Physics
Univ. of Tenn.
Knoxville, Tenn. 37916

Alan F. Haught
United Aircraft Corp.
Res. Labs
E. Hartford, Conn. 06108

John Hooper
School of EE
Georgia Inst. of Tech.
Atlanta, Ga. 30332

James P. Hurley
Univ. of Calif.
Dept. of Physics
Davis, Calif. 92110

Terry Kammash
Nuclear Engrg Dept
Univ. of Michigan
Ann Arbor, Mich. 48501

William Kehl
Dept. of Physics
Univ. of Calif., L.A.
Los Angeles, Calif. 90024

Donald E. Kerr
Dept. of Physics
Johns Hopkins University
Baltimore, Md. 21218

Donald W. Kerst
Sterling Hall
Dept. of Physics
Univ. of Wisconsin
Madison, Wisc. 53706

D. W. Koopman
Institute of Fluid Dynamics
Univ. of Md.
College Park, Md. 20740

Magna Kristiansen
Dept. of Physics
Texas Tech. College
Lubbock, Texas 79409

Arthur F. Kuckes
Cornell Univ.
Upson Hall
Ithaca, N.Y. 14850

H. J. Kunze
Inst. of Fluid Dynamics
Univ. of Md.
College Park, Md. 20740

Herbert Lashinsky
Inst. for Fluid Dynamics
& Applied Math
Univ. of Md.
College Park, Md. 20740

Laurence M. Lidsky
Dept. of EE
MIT
Cambridge, Mass. 02139

Charles Loepkey, Asst. Director
Computer Center
Univ. of Calif., Santa Barbara
Santa Barbara, Calif. 93105

Moshe Lubin, Jr.
College of Engrg & Applied Science
Univ. of Rochester
Rochester, N.Y. 14627

R. J. Madden
Natl. Bur. of Standards
Wash., D.C. 20234

A. MacKenzie
Dept. of Physics
Univ. of Calif., L.A.
Los Angeles, Calif. 90024

Tihiro Ohkawa
Gulf General Atomic Corp
P.O. Box 608
San Diego, Calif. 92112

Kenneth Rogers
Dept. of Physics
Stevens Inst. of Tech.
Hoboken, N.J. 07030

Harry S. Robertson
Dept. of Physics
University of Miami
Coral Gables, Fla. 33124

Anthony Robson
Univ. of Texas at Austin
Physics Dept.
Austin, Texas 78712

David J. Rose
Nuclear Engrg Dept
MIT
Cambridge, Mass. 02139

Marshall N. Rosenbluth
Inst. for Advanced Study
Princeton, N.J. 08540

Nathan Rynn
Dept. of Physics
Univ. of Calif.
Irvine, Calif. 92664

John Scharer
Dept. of Physics
Univ. of Wisconsin
Madison, Wisc. 53706

George Schmidt
Dept. of Physics
Stevens Inst. of Tech.
Hoboken, N.J. 07030

J. L. Shohet
Dept. of Physics
University of Wisconsin
Madison, Wisc. 53706

Albert Simon
Dept. of Physics
Univ. of Rochester
Rochester, N.Y. 14627

D. Gary Swanson
Dept. of Physics
Univ. of Texas
Austin, Texas 78712

D. A. Tidman
Univ. of Md.
Inst. for Fluid Dynamics
College Park, Md. 20740

Keith Thomassen - SEL
Stanford University
Stanford, Calif. 90024

William B. Thompson
Dept. of Physics
Univ. of Calif., San Diego
La Jolla, Calif. 90024

George Yevick
Dept. of Physics
Stevens Inst. of Tech.
Hoboken, N.J. 07030

Daniel R. Wells
Dept. of Physics
Univ. of Miami
Coral Gables, Fla. 33124

Jerry Weinstock
Inst. for Telecommunications, Sciences
& Aeronomy
Environmental Science Services Adm.
Boulder, Colo. 80303

C. B. Wharton
Lab. of Plasma Studies
Cornell Univ.
Ithaca, N.Y. 14850

A. Wong
Dept. of Physics
Univ. of Calif., L.A.
Los Angeles, Calif 90024